MAPPING THE BURNED AREA OF MULI FOREST FIRE USING MULTIPLE MACHINE LEARNING ALGORITHMS BASED ON LANDSAT-8 IMAGES

Chaoyu Huang[1] and Lin Xiao[1]
[1]Sichuan Agricultural University, Chengdu 611130, China, xiaolin@lzb.ac.cn

KEY WROKDS: Landsat-8; Gaofen-1; Machine Learning algorithm; Remote Sensing; Forest Fire

ABSTRACT: Forest fire is one of the most important disturbance of the world, which constantly affect the social and natural society. However, previous studies focused on mapping burned area on coarse spatial resolution satellite imagery generally shows low accuracy for small region because of the spatial heterogeneity. In this study, we compared the behavior of four different Machine Learning algorithms, Random Forest (RF), Support Vector Machine (SVM), k-Nearest Neighbor (kNN) and Naive Bayes (NB), in mapping the Muli forest fire occurred on 28 March 2020 (Liangshan, Sichuan, China) based on Landsat-8 and Gaofen-1 imagery. A feature importance based attribute selection was implemented using Random Forest algorithm to reduce the dimensionality of the data. To select the optimum parameters, models were trained using 70% of the database following a five-fold approach. We found that the predictors characterizing the difference between pre-fire and post-fire reflectance performed best. kNN and NB works more efficiently than the other two algorithms. Due to the distinctive spectral characteristics that burned area has, all of the Machine Learning algorithms showed similar spatial pattern. The best result was obtained by SVM (OA=0.9677, kappa = 0.9365), followed by RF (OA = 0.9672, kappa = 0.9345), KNN (OA=0.9670, kappa = 0.9340). NB showed the worst performance with OA is equal to 0.9442 and kappa coefficient is equal to 0.8861. The commission error ranged from 0.0325 to 0.0398, and omission error ranged from 0.0244 to 0.0831. Considering both computation time and accuracy, kNN maybe is the better way to map the burned area in Muli. Besides that, kNN mapped more burned area than other algorithms, which reached 16190 ha.

1. INTRODUCTION

Forest fires have been topical in the terrestrial ecosystem, causing an increase in atmospheric trace gas emission(Kloster et al. 2012; Ngadze et al. 2020; van der Werf et al. 2010), changing the distribution of the vegetation(Goldammer, Statheropoulos, and Andreae 2008) and having a great impact on social systems(Hawbaker et al. 2020). It is also regarded as an Essential Climate Variable (ECV) by the Global Climate Observing System (GCOS)(Hollmann et al. 2013). According to the Intergovernmental Panel on Climate Change (IPCC), human activity and the changes of climate tend to increase the risk of forest fires(Pacheco et al. 2021).

Accurately mapping the burned area is a vital approach to quantitatively analysis the influence of the wildfire, monitor vegetation recovery and understand the internal mechanism of wildfire(Polychronaki and Gitas 2012). The understanding of fire pattern in different environmental and climate conditions improves the management of sustainable forests(Chu and Guo 2014).

Burned area mapping methods can be divided into field investigation based and remote sensing based method. Compared to the former method, using satellite data is time and cost efficient with high temporal frequency(Knopp et al. 2020). Because the NIR and SWIR spectral regions are very sensitive to fire effects(García and Caselles 1991; Oliva, MartíN, and Chuvieco 2011; Pereira et al. 1999; Pleniou and Koutsias 2013; Trigg and Flasse 2001), satellite imagery based methods have shown good performance in generating burned area(Long et al. 2019). Previous Burned area products were mostly based on coarse resolution imagery, such as Moderate Resolution Imaging Spectroradiometer (MODIS) data, which is difficult to accurately mapping the Burned areas. The free availability of

Landsat-8 provides a chance for medium resolution burned area mapping(D. P. Roy et al. 2014; David P. Roy et al. 2019). Landsat data showed a strong ability to map small and spatially fragmented burned areas which is difficult to achieve with coarse resolution data(Laris 2005; Scholes, Kendall, and Justice 1996; Silva, Sá, and Pereira 2005). However, the Landsat-8 based burned area mapping is constrained by longer repeat cycle (16-day) and cloud obscuration(Alonso-Canas and Chuvieco 2015; Long et al. 2019; David P. Roy et al. 2019), which heavily affects the acquisition of high quality imagery. Thus, the traditional approaches applied to map burned area from coarse spatial resolution data do not perform well using Landsat-8 imagery(Long et al. 2019).

Burned area mapping is based on the changes of reflectance after fire(Chuvieco 2019). The quality of fire product is determined by the precision and reliability of satellite data, as well as the robustness of the algorithm. Among the algorithms used to generate burned area from Landsat imagery, Machine learning algorithms have been performing well(Knopp et al. 2020), such as Random Forest (RF)(Pacheco et al. 2021; Padilla et al. 2015; Ramo and Chuvieco 2017), Support Vector Machine (SVM)(Dragozi et al. 2014; Zhao, Huang, and Zhu 2015), k-Nearest Neighbor (kNN)(Pacheco et al. 2021), Naïve Bayes (NB)(Kern et al. 2017), classification and regression trees(Kontoes et al. 2009; Mallinis and Koutsias 2012), logistic regression(Koutsias and Karteris 1998), and K-means(Küçük Matcı and Avdan 2020), etc. Hence, Machine Learning algorithms are widely accepted in classifying burned areas.

Nevertheless, few studies have been done to map the burned area with high variation of terrain. The free availability of Landsat-8 and the using of Machine Learning algorithms allows for more reliable estimation and improves burned detection algorithms. Subsequently, this would also improve the evaluation of ecosystem damage and carbon emission.

The main objective of this study was to compare the capacity of four well-known machine learning algorithms, namely Random Forest (RF), Support Vector Machine (SVM), k-Nearest Neighbor (kNN) and Naïve Bayes (NB) to map the burned area of Muli using Landsat 8 scenes. The performance was evaluated by leaving 30% of the training database for independent validation. We select 6 Landsat bands and 7 priori spectral indices that are useful to distinguish the burned area, as inputs to train the Machine Learning algorithms. Then we imply a feature importance based feature selection to reduce the huge computation cost and generate a balanced Machine learning algorithm that maps burned area without overfitting or bias to the majority (or minority) class(Ramo et al. 2018). We use four kind of metrics, namely overall accuracy (OA), omission error (OE), commission error (CE) and kappa coefficient to access the model performance.

2.STUDY AREA

The study area is located in the southeast of Muli, Sichuan, China, which is largely rural and has complex terrain and climate conditions. Muli is rich in forest resources, the forest cover rate of Muli reaches 67.3%. And the main tree species include *Picea asperata, Quercus semecarpifolia, Pinus densata,* etc. Because of the wideness of forest and the treacherous terrain, it is more difficult to control the fire than other place. According to the history of forest fire in Muli, the period of fire prevention mainly between December to June. With the onset of the rainy season, the probability of wildfire immediately decreases.

The burned area (Figure 1) covers a fire around 160 km^2 that started on March 28 and ended on April 6 in the southeast of Muli. Though the main characteristic of forest fires that happen on alpine area is always small and frequent, with the effect of strong and erratic winds, this fire happened in Muli caused a large area destroyed and several deaths. As a result, a variety of land cover types was changed and present different properties after fire which introduce difficulties in mapping burned area.

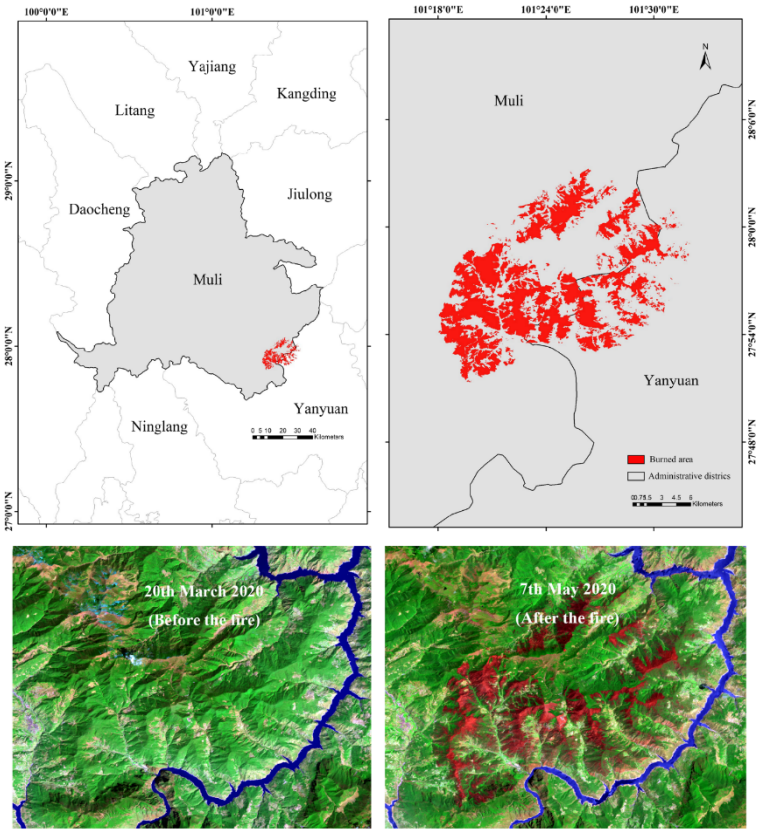

Figure 1. Location of the study area at Muli (Sichuan, China). The analyzed burned area is represented on the right map with a red pattern. At the bottom are two satellite images from Landsat 8, corresponding to the scenes of 20 March 2020 (LC08_L1TP_131041_20200320_20200326_01_T1), before the fire, and 7 May 2020 (LC08_L1TP_131041_20200507_20200509_01_T1), after the fire.

3. MATERIALS AND METHODS

3.1 Satellite data

BA mapping: We used one Landsat 8 OLI/TIRS image before and one after fire, respectively on Mach 20 and May 7. Both of them were downloaded from the archive of the USGS earth Resources Observation and Science Center (https://earthexplorer.usgs.gov/) which provides images processed with the Standard Terrain Correction (L1TP). We use the Radiometric Calibration tool in ENVI 5.3 to calibrate the digital numbers (DN) to surface reflectance.

BA validation: Commonly, when satellite data are used as reference data, they should have higher spatial resolution than the data used to generate the BA product(Long et al. 2019). We used one Gaofen-2 imagery to validate the Landsat data. The characteristics of GF1 are illustrated in Table 1.

Table 1. Landsat OLI and Gaofen PMS bands used by the Machine Learning algorithms. NIR: near infrared, SWIR: shortwave infrared

Band name	Landsat OLI		Gaofen-1 PMS	
	wavelength	spatial resolution	wavelength	spatial resolution
Blue	0.45-0.51	30	0.45-0.52	8
Green	0.53-0.59	30	0.52-0.59	8
Red	0.64-0.67	30	0.63-0.69	8
NIR	0.85-0.88	30	0.77-0.89	8
SWIR 1	1.57-1.65	30		
SWIR 2	2.11-2.29	30		

3.2 Method

The methodology applied in this study is consisted of several steps, including the training datasets compilation, feature selection, Machine Learning algorithms training and accuracy analysis.

3.2.1 Training and Validation datasets: In the BA algorithm, we include six Landsat bands and 7 more spectral indices (Table2) that showed good performance in previous studies. The pre-fire indices showed the surface conditions before fire. The post-fire indices showed the re We use Landsat-8 archive to generate the BA product. Because of its higher spatial resolution, we use Gaofen-2 imagery as reference data.

Table 2. The formulas of spectral indices that are sensitive to burned areas.

Name	Abbreviation	Formula	Reference
Normalized Difference Vegetation Index	NDVI	$\frac{\rho NIR - \rho RED}{\rho NIR + \rho RED}$	Stroppiana et al.(Stroppiana et al. 2009)
Soil-Adjusted Vegetation Index	SAVI	$\frac{(1+0.5)(\rho NIR - \rho RED}{\rho NIR + \rho RED + 0.5}$	huete(Huete 1988)
Normalized Burned Ratio	NBR	$\frac{\rho NIR - \rho SWIR2}{\rho NIR + \rho SWIR2}$	Key and Benson(Key and Benson 2003)
Normalized Burned Ratio 2	NBR2	$\frac{\rho SWIR1 - \rho SWIR2}{\rho SWIR1 + \rho SWIR2}$	Lutes et al.((PDF) FIREMON n.d.)
Normalized Difference MOisture Index	NDMI	$\frac{\rho NIR - \rho SWIR1}{\rho NIR + \rho SWIR1}$	Wilson and Sader(Wilson and Sader 2002)
NIR/red ratio	VI43	NIR/Red	Tucker(Tucker 1979)
SWIR1/SWIR2 ratio	VI57	SWIR1/SWIR2	Epting(Epting, Verbyla, and Sorbel 2005)

3.2.2 Feature selection: We use feature selection (FS) to reduce the dimensionality of dataset and cut the cost of computation by removing redundant features. Besides, it can also help to reduce the risk of overfitting. We used a RF based approach to select the most important attributes used in algorithm.

3.2.3 Machine learning algorithms: To delineate the burned area of Muli, we used four kind of common machine learning algorithms which have shown significant performance in the previous study.

The first algorithm applied was a support vector machine(SVM), which was developed by Vanpnik(Boser, Guyon, and Vapnik 1992). It is designed to find an optimal hyperplane to classify the dataset. In this study, the kernel of SVM we used was a radial basis function. And the accuracy of the algorithm is determined by two parameters, g and C.

The second algorithm applied was a Random Forest Classifier (RF) which was proposed by Leo Breiman(Breiman 2001) in 2001. As one of the most popular algorithm used in remote sensing domain, RF has also been used to predict fire occurrence(Oliveira et al. 2012), characterize fire regime(Aldersley, Murray, and Cornell 2011; Archibald et al. 2009) and map burned area(Long et al. 2019; Ramo et al. 2018).

The third algorithm applied was a k-Nearest Neighbor Classifier (kNN), which was proposed by Aha. kNN is a popular algorithm used in remote sensing data mining(Pacheco et al. 2021), and it also performed well in mapping burned area. The parameter k which represents the chosen number of closest neighbor determines the accuracy of the algorithm.

The forth algorithm applied was a Naïve Bayes (NB), which is based on applying Bayes theorem with the naïve assumption of conditional independence(Naïve Bayes Author: Geoffrey I Webb, Monash University Synonyms Idiot's Bayes, Simple Bayes Definition Naïve Bayes is a simp n.d.). It is simple and efficient.

3.2.4 Accuracy analysis: In this work, we use a confusion matrix (Table 3) to analysis the performance of all kind of algorithms we used. When the reference data and the classified result are all positive, it will be counted as a true positive (TP). When the reference data and the classified result are all negative, it will be counted as a true negative (TN). When the reference data is positive and the classified result is negative, it will be counted as a false negative (FN). And when the reference data is negative and the classified result is positive, it will be counted as a false positive (FP).

Table 3. The confusion matrix made by reference data and classified results.

		Reference data(pixel)		
		Burned	Unburned	Total
Classified results(pixel)	Burned	TP	FP	TP+FP
	Unburned	FN	TN	FN+TN
	Total	TP+FN	FP+TN	TP+FN+FP+TN

The confusion matrix clearly showed the difference between the reference data and the classified results. It helps us to derive four statistical parameters, i.e., overall accuracy (OA), commission error (CE), omission error (OE) and kappa coefficient (K).

4. RESULTS

4.1 Feature selection

The attribute selection used in this study depends on feature importance. The final attribute selection is composed by 14 different features. Eight of the selected variables are based on the difference between the post and the pre-fire signals while six of them corresponds to the post-fire scenario.

4.2 Mahine Learning Algorithm Training

4.2.1 NB Training: We used GaussianNB and BernoulliNB to map the Muli burned area. Both of them cost less time to compute compared with other algorithms, but performed bad.

Table 1. The training result of GaussianNB and BernoulliNB.

	GaussianNB	BernoulliNB
accuracy	0.9442	0.9340

4.2.2 RF Training: Figure 1 shows the change of accuracy for a different number of trees from 20 to 400. It shows that, with the increases of tree number, the accuracy increases first then tends to be stable. It can be seen that 260 is the best value for trees.

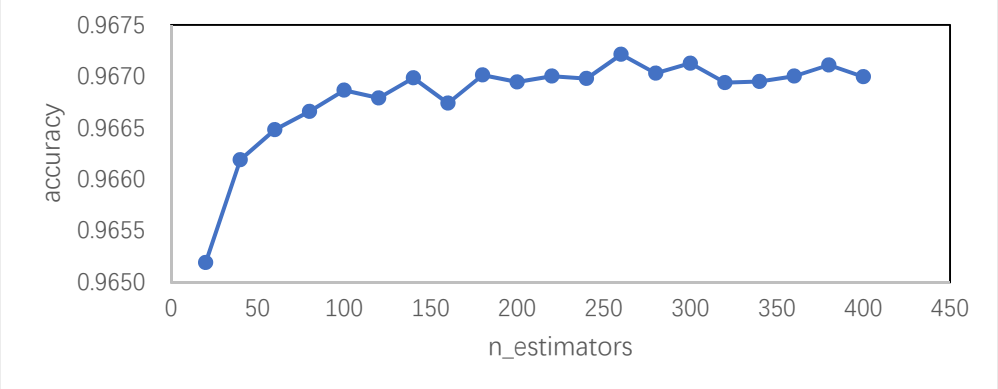

Figure 2. The training result of RF classifier.

4.2.3 kNN Training: In this study, we tested different k values (5 to 50) to acquire the optimal kNN classifier. From figure 2 we can see that, the accuracy increase first and then decreases with the increase of k value. And the best k value to map the Muli burned area is 25.

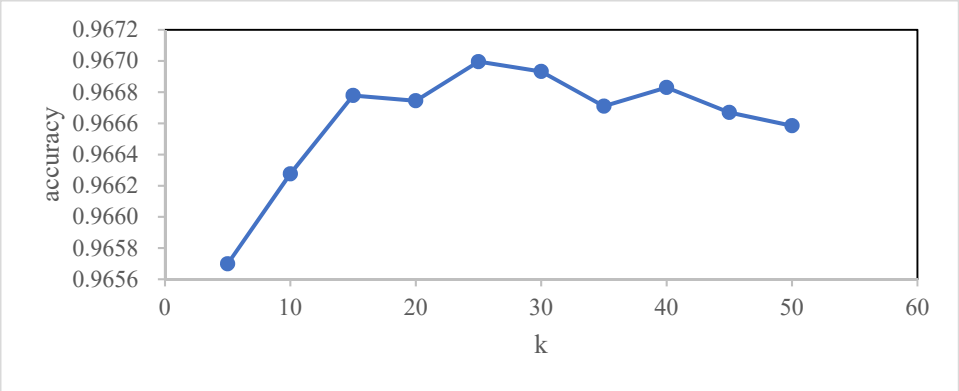

Figure 3. The training result of kNN.

4.2.4 SVM Training: The accuracy of SVM is controlled by two parameters, c and gamma. With the increase of c and gamma, the accuracy increases first and then decreases after. When c is equal to 10 and gamma is equal to 1, the algorithm performed best.

c \ gamma	0.01	0.1	1	10	100
0.01	0.9603	0.9636	0.9639	0.9169	0.5005
0.1	0.9626	0.9650	0.9661	0.9434	0.5009
1	0.9642	0.9656	0.9672	0.9626	0.8133
10	0.9651	0.9663	0.9677	0.9555	0.8195
100	0.9658	0.9668	0.9661	0.9538	0.8195

Figure 4. The training result of SVM.

4.3 Algorithm evaluation

Table 2 shows the commission error, omission error, kappa coefficient and accuracy computed based on the remaining 30% of the training dataset that used to carry out a cross-tabulation:

The best accuracy was obtained by the SVM followed by kNN and RF. NB showed the highest commission error and omission error. And kNN had a good performance with low computation cost. On the other hand, kNN mapped more burned area than other algorithms.

Table 2. The commission error, omission error, kappa coefficient and accuracy of four kind of Machine Learning algorithms.

	SVM	RF	kNN	NB
commission error	0.0385	0.0370	0.0398	0.0325
omission error	0.0244	0.0281	0.0256	0.0831
Kappa coefficient	0.9365	0.9345	0.9340	0.8861
accuracy	0.9677	0.9669	0.9670	0.9442
area(ha)	16107	15,911	16190	15,361

4.4 Burned Area Analysis

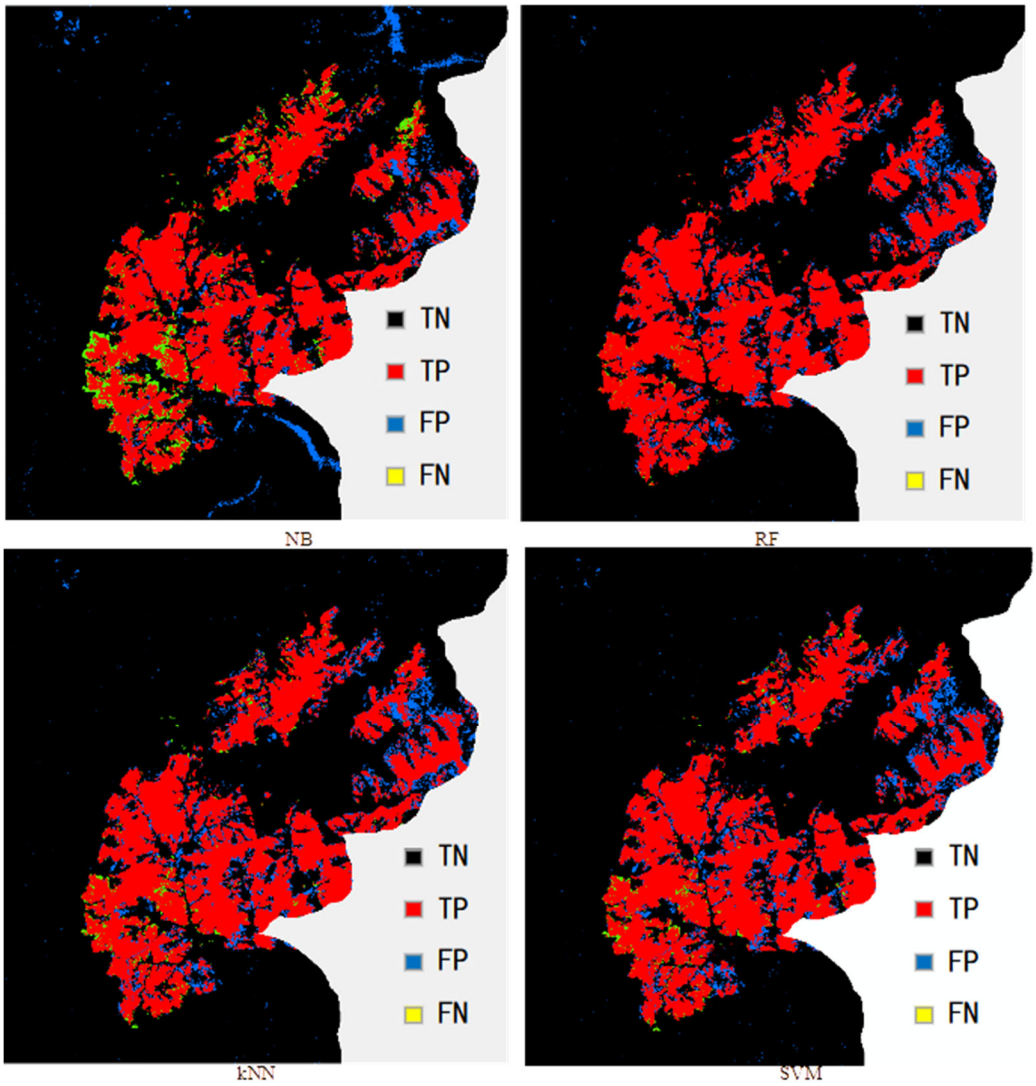

Figure 5. The black area shows the true negative pixels; The red area shows the true positive areas; The blue area shows the false positive area; The yellow area shows the false negative pixels.

Figure 5 shows that all of the algorithms have similar spatial pattern. We can see that RF has little area that recognized as false negative pixels. And NB has more pixels falsely delineation than other algorithms. On the top left corner, all of the training results appear a lot of false positive pixels. This phenomenon occurred is because of the particularity of land cover type and relative coarse spatial resolution that Landsat-8 has.

5. DISCUSSION

5.1. Feature selection

Feature selection helps to reduce the dimensionality if data and computation cost. The feature importance based RF filter gave more importance to bands difference and post-fire reflectance. We select those features whose feature importance is larger than 0.04. The most important attribute is NBR difference, followed by NBR2 difference, NDVI difference, SAVI difference, NDMI difference, SAVI post, NDVI post, NBR2 post, NIR difference, NDMI post, SWIR2 difference, MIRBI difference, GEMI post, NBR post. The pre-fire information is relatively unimportant. We can see that spectral indices made sense to map the forest fire.

5.2. Model training

The training dataset was composed of 250,056 pixels which made it relatively large. This means the computation cost is considerably high. Although the feature selection reduced the dimensionality of dataset, the SVM and RF classifier spent a lot of time in computing. We used a 5-fold cross validation approach to acquire the best parameter. The 5-fold cross validation made better estimation by averaging the different partitions.

5.3. Model evaluation

We evaluated the performance of models by remaining 30% of the training dataset. SVM, RF and kNN showed very good performance, with omission and commission errors less than 0.03 and 0.04, respectively. The NB classifier missed a lot of burned pixels, with omission error is equal to 0.08. Although the best result was obtained by SVM, we prefer the kNN classifier because of its low computation cost and considerable performance.

Although we put a lot of effort in the study, some difficulties still remained. For example, the burned conditions are very different which resulted in varies reflectance change and difficult to accurately map the burned area. Because of the relatively coarse resolution Landsat-8 has, the accuracy was largely effected by the mixed pixels which was not completely burned. Each algorithm also has its own requirements that have to be considered. For instance, SVM works very slow when the dataset is very large, but it has the best performance.

6. CONCLUSIONS

This paper evaluated the ability of RF, kNN, SVM and NB to map the burned area in Muli, following a feature and parameter selection. The feature selection was based on the feature importance, which reduced the dimensionality of dataset and computation cost. The most important features were related to the temporal difference of spectral indices and post-fire conditions. We used a 5-fold cross validation to prevent the overfitting of Machine learning algorithms. SVM, RF and kNN showed very good performance, with omission and commission error were less than 0.03 and 0.04. The NB classifier missed a lot of burned pixels which resulted in its large omission error. We prefer the kNN classifier in mapping the burned area in Muli, because of its considerable performance and relatively low computation cost.

References

Aldersley, Andrew, Steven J. Murray, and Sarah E. Cornell. 2011. Global and Regional Analysis of Climate and Human Drivers of Wildfire. Science of The Total Environment, 409(18), pp. 3472–81

Alonso-Canas, Itziar, and Emilio Chuvieco. 2015. Global Burned Area Mapping from ENVISAT-MERIS and MODIS Active Fire Data. Remote Sensing of Environment, 163, pp. 140–52.

Archibald, Sally, David P. Roy, Brian W. Van WILGEN, and Robert J. Scholes. 2009. What Limits Fire? An Examination of Drivers of Burnt Area in Southern Africa. Global Change Biology, 15(3), pp. 613–30.

Boser, Bernhard E., Isabelle M. Guyon, and Vladimir N. Vapnik. 1992. A Training Algorithm for Optimal Margin Classifiers. In Proceedings of the Fifth Annual Workshop on Computational Learning Theory, COLT '92, New York, NY, USA: Association for Computing Machinery, pp. 144–52.

Breiman, Leo. 2001. "Random Forests." Machine Learning, 45(1), pp. 5–32.

Chu, Thuan, and Xulin Guo. 2014. Remote Sensing Techniques in Monitoring Post-Fire Effects and Patterns of Forest Recovery in Boreal Forest Regions: A Review. Remote Sensing, 6(1), pp. 470–520.

Chuvieco, Emilio. 2019. Historical Background and Current Developments for Mapping Burned Area from Satellite Earth Observation. Remote Sensing of Environment, pp. 20.

Dragozi, Eleni, Ioannis Z. Gitas, Dimitris G. Stavrakoudis, and John B. Theocharis. 2014. Burned Area Mapping Using Support Vector Machines and the FuzCoC Feature Selection Method on VHR IKONOS Imagery. Remote Sensing, 6(12) pp. 12005–36.

Epting, Justin, David Verbyla, and Brian Sorbel. 2005. Evaluation of Remotely Sensed Indices for Assessing Burn Severity in Interior Alaska Using Landsat TM and ETM+. Remote Sensing of Environment, 96(3), pp. 328–39.
García, M.J. López, and V. Caselles. 1991. Mapping Burns and Natural Reforestation Using Thematic Mapper Data. Geocarto International, 6(1), pp. 31–37.
Goldammer, Johann G., Milt Statheropoulos, and Meinrat O. Andreae. 2008. Chapter 1 Impacts of Vegetation Fire Emissions on the Environment, Human Health, and Security: A Global Perspective. In Developments in Environmental Science, Wildland Fires and Air Pollution, eds. Andrzej Bytnerowicz, Michael J. Arbaugh, Allen R. Riebau, and Christian Andersen. Elsevier, pp. 3–36.
Hawbaker, Todd J. et al. 2020. The Landsat Burned Area Algorithm and Products for the Conterminous United States. Remote Sensing of Environment, pp. 244: 111801.
Hollmann, R. et al. 2013. The ESA Climate Change Initiative: Satellite Data Records for Essential Climate Variables. Bulletin of the American Meteorological Society, 94(10), pp. 1541–52.
Huete, A. R. 1988. A Soil-Adjusted Vegetation Index (SAVI). Remote Sensing of Environment, 25(3), pp. 295–309.
Kern, Ashley N. et al. 2017. Machine Learning Based Predictive Modeling of Debris Flow Probability Following Wildfire in the Intermountain Western United States. Mathematical Geosciences, 49(6), pp. 717–35.
Key, Carl H.; Benson, Nathan C. 2003. The normalized burn ratio (NBR): a Landsat TM radiometric measure of burn severity (Abstract). US Geological Survey Northern Rocky Mountain Science Center, U.S. Department of the Interior.
Kloster, S., N. M. Mahowald, J. T. Randerson, and P. J. Lawrence. 2012. The Impacts of Climate, Land Use, and Demography on Fires during the 21st Century Simulated by CLM-CN. Biogeosciences, 9(1), pp. 509–25.
Knopp, Lisa, Marc Wieland, Michaela Rättich, and Sandro Martinis. 2020. A Deep Learning Approach for Burned Area Segmentation with Sentinel-2 Data. Remote Sensing, 12(15), pp. 2422.
Kontoes, C. C. et al. 2009. A Comparative Analysis of a Fixed Thresholding vs. a Classification Tree Approach for Operational Burn Scar Detection and Mapping. International Journal of Applied Earth Observation and Geoinformation, 11(5), pp. 299–316.
Koutsias, N., and M. Karteris. 1998. Logistic Regression Modelling of Multitemporal Thematic Mapper Data for Burned Area Mapping. International Journal of Remote Sensing, 19(18), pp. 3499–3514.
Küçük Matcı, Dilek, and Uğur Avdan. 2020. Comparative Analysis of Unsupervised Classification Methods for Mapping Burned Forest Areas. Arabian Journal of Geosciences, 13(15), pp. 711.
Laris, Paul S. 2005. Spatiotemporal Problems with Detecting and Mapping Mosaic Fire Regimes with Coarse-Resolution Satellite Data in Savanna Environments. Remote Sensing of Environment, 99(4), pp. 412–24.
Long, Tengfei et al. 2019. 30 m Resolution Global Annual Burned Area Mapping Based on Landsat Images and Google Earth Engine. Remote Sensing, 11(5), pp. 489.
Mallinis, Giorgos, and Nikos Koutsias. 2012. Comparing Ten Classification Methods for Burned Area Mapping in a Mediterranean Environment Using Landsat TM Satellite Data. International Journal of Remote Sensing 33(14), pp. 4408–33.
Ngadze, Fiona et al. 2020. Exploring the Utility of Sentinel-2 MSI and Landsat 8 OLI in Burned Area Mapping for a Heterogenous Savannah Landscape. PLOS ONE 15(5).
Oliva, P., P. MartíN, and E. Chuvieco. 2011. Burned Area Mapping with MERIS Post-Fire Image. International Journal of Remote Sensing, 32(15), pp. 4175–4201.
Oliveira, Sandra et al. 2012. Modeling Spatial Patterns of Fire Occurrence in Mediterranean Europe Using Multiple Regression and Random Forest. Forest Ecology and Management, pp. 275: 117–29.
Pacheco, Admilson da Penha, Juarez Antonio da Silva Junior, Antonio Miguel Ruiz-Armenteros, and Renato Filipe Faria Henriques. 2021. Assessment of K-Nearest Neighbor and Random Forest Classifiers for Mapping Forest Fire Areas in Central Portugal Using Landsat-8, Sentinel-2, and Terra Imagery. Remote Sensing, 13(7), pp. 1345.
Padilla, Marc et al. 2015. Comparing the Accuracies of Remote Sensing Global Burned Area Products Using Stratified

Random Sampling and Estimation. Remote Sensing of Environment, 160, pp. 114–21.
Pereira, José M. C. et al. 1999. Spectral Characterisation and Discrimination of Burnt Areas. In Remote Sensing of Large Wildfires: In the European Mediterranean Basin, ed. Emilio Chuvieco. Berlin, Heidelberg: Springer, pp. 123–38.
Pleniou, Magdalini, and Nikos Koutsias. 2013. Sensitivity of Spectral Reflectance Values to Different Burn and Vegetation Ratios: A Multi-Scale Approach Applied in a Fire Affected Area. ISPRS Journal of Photogrammetry and Remote Sensing, 79, pp. 199–210.
Polychronaki, Anastasia, and Ioannis Z. Gitas. 2012. Burned Area Mapping in Greece Using SPOT-4 HRVIR Images and Object-Based Image Analysis. Remote Sensing, 4(2), pp. 424–38.
Ramo, Rubén, and Emilio Chuvieco. 2017. Developing a Random Forest Algorithm for MODIS Global Burned Area Classification. Remote Sensing, 9(11), pp. 1193.
Ramo, Rubén, Mariano García, Daniel Rodríguez, and Emilio Chuvieco. 2018. A Data Mining Approach for Global Burned Area Mapping. International Journal of Applied Earth Observation and Geoinformation, 73, pp. 39–51.
Roy, D. P. et al. 2014. Landsat-8: Science and Product Vision for Terrestrial Global Change Research. Remote Sensing of Environment, 145, pp. 154–72.
Roy, David P. et al. 2019. Landsat-8 and Sentinel-2 Burned Area Mapping - A Combined Sensor Multi-Temporal Change Detection Approach. Remote Sensing of Environment, 231, pp. 111254.
Scholes, R. J., J. Kendall, and C. O. Justice. 1996. The Quantity of Biomass Burned in Southern Africa. Journal of Geophysical Research: Atmospheres, 101(D19), pp. 23667–76.
Silva, João M. N., Ana C. L. Sá, and José M. C. Pereira. 2005. Comparison of Burned Area Estimates Derived from SPOT-VEGETATION and Landsat ETM+ Data in Africa: Influence of Spatial Pattern and Vegetation Type. Remote Sensing of Environment, 96(2), pp. 188–201.
Stroppiana, D., M. Boschetti, P. Zaffaroni, and P. A. Brivio. 2009. Analysis and Interpretation of Spectral Indices for Soft Multicriteria Burned-Area Mapping in Mediterranean Regions. IEEE Geoscience and Remote Sensing Letters, 6(3), pp. 499–503.
Trigg, S., and S. Flasse. 2001. An Evaluation of Different Bi-Spectral Spaces for Discriminating Burned Shrub-Savannah. International Journal of Remote Sensing, 22(13), pp. 2641–47.
Tucker, Compton J. 1979. Red and Photographic Infrared Linear Combinations for Monitoring Vegetation. Remote Sensing of Environment, 8(2), pp. 127–50.
van der Werf, G. R. et al. 2010. Global Fire Emissions and the Contribution of Deforestation, Savanna, Forest, Agricultural, and Peat Fires (1997–2009). Atmospheric Chemistry and Physics, 10(23), pp. 11707–35.
Wilson, Emily Hoffhine, and Steven A Sader. 2002. Detection of Forest Harvest Type Using Multiple Dates of Landsat TM Imagery. Remote Sensing of Environment, 80(3), pp. 385–96.
Zhao, Feng, Chengquan Huang, and Zhiliang Zhu. 2015. Use of Vegetation Change Tracker and Support Vector Machine to Map Disturbance Types in Greater Yellowstone Ecosystems in a 1984–2010 Landsat Time Series. IEEE Geoscience and Remote Sensing Letters, 12(8), pp. 1650–54.